Mineralogical Magazine, October 2006, Vol. 70(5), pp. 485–498

Agate and chalcedony from igneous and sedimentary hosts aged from 13 to 3480 Ma: a cathodoluminescence study

T. MOXON[1,*] AND S. J. B. REED[2]

[1] 55 Common Lane, Auckley, Doncaster DN9 3HX, UK
[2] Department of Earth Sciences, University of Cambridge, Downing Street, Cambridge CB2 3EQ, UK

ABSTRACT

Chalcedony and agates from a variety of world-wide hosts have been examined using cathodoluminescence (CL). Gaussian fitting of the experimental data shows that there are two dominant spectral emissions at ~400 and ~660 nm. A third subordinate peak is also found at ~470, ~560 or ~620 nm. An age-related link is shown between the respective decreasing and increasing relative intensities of the 660 and 620 nm emissions. It is proposed that this change is due to a condensation reaction between neighbouring Si–OH groups eliminating water and forming a strained Si–O–Si bond.

Agates from a variety of hosts and regions produced no clear demonstrable CL distinctions. However, a set of Western Australian agates was examined from host rocks that had been subjected to burial metamorphism. Cathodoluminescence produced different spectral emissions in the petrographic fibrous and granular regions of these agates. One agate shows a partial transformation of the petrographic fibrosity into granularity. This conversion is characterized by emission bands at 570 nm and 460 nm. Similar emission-band changes were produced by heating Brazilian agates for 35 days at 300ºC. The identification of these changes in agate could serve as an indicator of palaeoheating within the parent rock.

KEYWORDS: agate, chalcedony, cathodoluminescence, age, silanol, water.

Introduction

MICROCRYSTALLINE quartz is generally classified by its petrographic characteristics. Chert usually shows a granular microstructure while chalcedony is the fibrous variety of α-quartz; banded chalcedony is known as agate. Agate with banding in concentric zones is defined as wall-lining agate. The banding is caused by various occurrences: Fe oxide spots, apparent pauses in the crystallization process and textural changes. Less often, agate appears as horizontal banding that is presumed to have been gravity-controlled. Agates are most frequently found within a variety of fine-grained volcanic host rocks. Sedimentary hosts are less abundant but agates have been found in limestone, e.g. the Minnelusa Formation, South Dakota, USA (Clark, 2002).

Agate has a high silica purity that is generally >97% with non-volatile impurities <1% (Flörke *et al*., 1982). The total water (H_2O and Si-OH groups) is the major impurity with a concentration up to 2% (Graetsch *et al*., 1985). However, most agate is a mixture of two silica polymorphs: α-quartz and moganite. The crystal structure of moganite has been described as the alternate stacking of layers of left- and right-handed quartz on the unit-cell scale (Miehe and Graetsch, 1992). Moganite was eventually acknowledged as an independent polymorph of silica in 1999 (IMA No 99-035).

The moganite content in agate can be as high as 20% (Heaney and Post, 1992). Moxon and Ríos (2004) showed that both the moganite and defect-site water in agate decreased with age during the first 400 Ma. Over the same time scale, the crystallite size of α-quartz grew by ~55%. For the

* E-mail: moxon.t@tiscali.co.uk
DOI: 10.1180/0026461067050347

next ~400 to 1100 Ma the crystallite size and the defect-site water was shown to be approximately constant. Agates from hosts >400 Ma old had, as detected by X-ray diffraction, trace moganite. In the same study, it was argued that the cessation of crystallite growth is due to the completion of a moganite → chalcedony transformation. However, advanced recrystallization has been found in agates from a 3480 Ma host in the Pilbara Craton, Western Australia (Moxon *et al.*, 2006).

Agate occurs on every continent but an understanding of agate genesis has proved to be problematic. Likely origins are either the direct precipitation of chalcedony or the deposition of amorphous silica (gel or powder) that matures into chalcedony. Agate has not been made in laboratory time and unsolved problems include the method of silica transportation and deposition, together with the mechanism of crystallization. The majority of recent workers would accept that agates form at temperatures <100ºC (Heaney, 1993).

Cathodoluminescence (light emission stimulated by electron bombardment) of quartz has various causes: CL spectra may include lines, usually associated with particular elements, and bands related to various types of crystal defects, but only the latter are observed in the case of agate. Sharp emission lines are not generally shown by quartz and other silica polymorphs as the ions that produce these lines (e.g. *REE*, Cr^{3+}) are not incorporated into the quartz structure. Quartz CL has been investigated by many workers (Götze *et al*., 2001, and references therein). Studies of agate using CL are limited to the work of Götze *et al.* (1998, 1999) who identified three emission bands: a blue band (assigned to the $[AlO_4/M^+]$ to $[AlO_4]^0$ transition); a yellow band (related to intrinsic defects), and a red band attributed to non-bridging oxygen hole centres (NBOHC).

The prime aim of the present study was to investigate whether agate lattice defects, as detected by CL, would show any age-related or regional or host-rock differences. Banding in agates from sedimentary hosts is frequently seen as a 'holly-leaf' pattern; this suggests that genesis is different from the wall-lining agates of igneous hosts. Limestone-hosted agates from South Dakota, USA and chalcedony from Lyme Regis, England, were also included in the study. A final CL age comparison was made with agates found in Western Australian Proterozoic and Archaean hosts.

Agates from Brazil and Northumbria, England, are found in hosts that have been radiometrically dated at 133 and 391 Ma, respectively. However, the physical properties of agates from these regions suggest a younger agate genesis. Volcanic activity occurred in these areas at 80 and 167 Ma, respectively. It was proposed that these agates formed during this later period (Moxon and Ríos, 2004). The same study showed that, apart from the Brazilian and Northumbrian agates, there was a good correlation ($r_{58} = 0.79$) between crystallite size and hosts that were <400 Ma old. In general, the formation of wall-lining agate can be regarded as occurring within a few million years of the host.

Throughout the paper, data in parentheses are ± one standard deviation. Unless stated to the contrary, reference to agate also includes the described chalcedony. All error bars are ± one standard deviation.

Agate samples

More than 40 samples of agate were investigated from igneous hosts that range in age from 13 to 1100 Ma (Table 1). Apart from two samples of chalcedony, all the igneous-hosted agate was of the wall-lining type. Chalcedony from the Yucca Mt., USA (13 Ma) and Mt. Warning Shield Volcano, Queensland, Australia (23 Ma) were used because of their young host-rock age. Additional investigations included agates from three regions found in the Proterozoic and Archaean hosts, Western Australia. A further sample of a 1900 y old siliceous sinter (Lynne *et al*., 2005) served as a reference material of comparatively recently formed granular α-quartz.

Sedimentary agates from the Minnelusa limestone in South Dakota, USA were examined. The limestone formation circles the Black Hills and the eight agate samples used in the study were from a variety of sites >90 km apart. Lyme Regis chalcedony is found within the Cretaceous limestone of Lyme Bay, England. The chalcedony is an attractive mauve material with weak white banding but the botryoidal nature shows that it is a fissure infill (Fig. 1).

Experimental methods

Sample preparation

Slabs of agate, $\sim 1 \times 2.5 \times 0.3$ cm, were cut approximately parallel to the fibrous growth and ground flat with silicon carbide grit. All samples

TABLE 1. Agate samples used for CL.

Region	Age of host (Ma)	Host rock	Site and sample number (collector named in the Acknowledgements)
Igneous hosts			
1. Yucca Mt., USA	13[c]	Volcanic tuffs	Yucca Mt.: HD 2257 (LN)
2. Mt. Warning, Queensland, Australia	23[c]	Basalt	Oxley River: Tw2, 4, 7 (JRi)
3. Chihuahua, Mexico	38[g]	Andesite	Ojo Laguna: M5, 10, 13 (BC)
4. Khur, Iran	50[a]	Andesite	Khur: 7, 31, 33 (MN)
5. British Tertiary Volcanic Province	60[a]	Mugearite Basalt	Mull: 2, 14; Rhum: 5, 12, 15 (BT, RL)
6. Rio Grande do Sul, Brazil	133[a]	Basalt	Soledado Mines: B21, 25, 31, 33, 36, 60, 62, 64 (purchased)
7. Semolale, Botswana	180[c]	Basalt	Bobonong: 101, 110, 120, 80 (HK)
8. Agate Creek, Queensland, Australia	275[a]	Basalt	Agate Cr': 16, 65, 104, 129 (NC)
9. Thuringia, Germany	285[a]	Rhyolite	Thuringia Forest: Th 4 (GH)
10. Northumbria, England	391[a]	Andesite	R. Breamish: N49 (TM)
11. Eastern Midland Valley, Scotland	412[a]	Andesite	Ethiebeaton Q: 11, 37 (BW) Barras Q: 1 (BL)
12. Western Midland Valley, Scotland	412[a]	Basalt	Car' Hills: BC9, B Anne 3 (JRa)
13. Northern Terr', Australia	513[b]	Basalt	Antrim basalts: NT5 (JRi)
14. Lake Superior, USA	1100[a]	Basalt	Lincoln: 1, 4, 8 (BC) Minneapolis: 12, 14 (SW)
15. Killara, Western Australia	1840[c]	Dolerite	Killara Formation: K4, K6 (DN)
16. Maddina, Western Australia	2720[c]	Basalt	Maddina Basalt: M1 (DN)
17. Warrawoona, Western Australia	3480[c]	Rhyolite tuff	Warrawoona Group: W1 (DN)
Sinter deposit			
19. Sinter, Utah, USA	1900 y[d]		Utah: S1 (JM)
Sedimentary hosts			
20. Lyme Regis, England	105[e]	Limestone	Lyme Bay: LR1, 2, 3 (IL)
21. Fairburn, S. Dakota, USA	295[f]	Limestone	F: 1, 52; TP 7, 45; P95, 96, 101; CP17 (RC).

Age references are given in [a] Moxon (2002), [b] Moxon and Ríos (2004), [c] Moxon *et al.* (2006), [d] Lynne *et al.* (2005)
[e] The host formed during the Albian Stage (House, 1989). A mid-point has been used.
[f] The limestone host is Pennsylvanian to Lower Permian (Gries and Martin, 1985). A mid-point has been used.
[g] Keller *et al*. (1982)

were finally polished with 1 μm diamond paste and thinly coated with gold. Most agates were examined as slabs, but, in order to study the effect of CL on areas of changing fibrosity, 12 agates were investigated as polished thin sections. Markers, using diamond bit drilling, were made along the length of the samples. At least four wavelength scans were made at random points on each agate with extra scans on the varied petrographic features.

During the study it was found that age-related changes were possibly linked to a dehydration process. In order to investigate this possibility, two slabs each of agate from Brazil 60 and Brazil 64 were polished and marked by diamond drilling in three equidistant positions. Wavelength scans were carried out on the samples at the start and after dry-furnace heating at 300ºC for 35 and 56 days. After heating, the agates were re-coated with gold before re-examination with CL.

The available free and total water present in Brazil 60 and Brazil 64 were found by heating <52 μm powder samples in triplicate at 170ºC and 1200ºC, respectively. For details of the method, the reader is referred to Moxon and Ríos (2004).

Experimental

Cathodoluminescence spectra were recorded with a Gatan MonoCL3 system attached to a JEOL 820

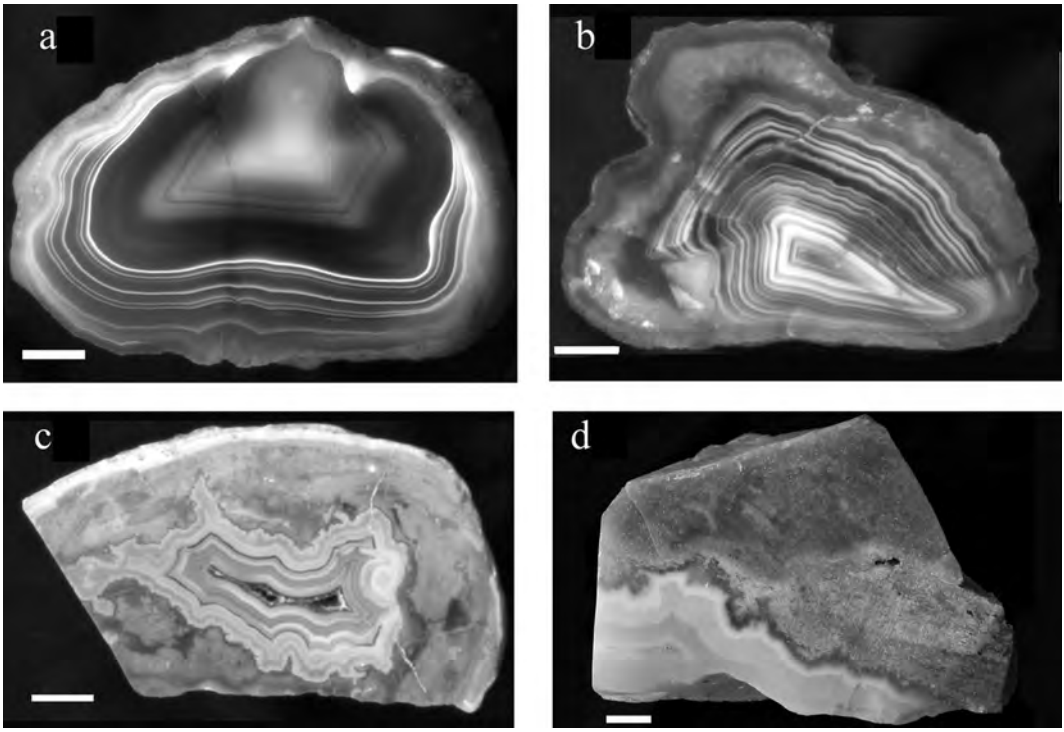

FIG. 1. (*a*) Wall-lining agate from Botswana. (*b*) Wall-lining agate from Ethiebeaton, Scotland. (*c*) Fairburn agate from the Pringle area, South Dakota, USA, showing the holly-leaf effect. (*d*) Vein chalcedony from Lyme Regis, England. Scale bars: 1 cm.

scanning electron microscope, using the following conditions: accelerating voltage: 20 kV, beam current: ~10 nA, spot size: ~10 µm. Light collected by a paraboloidal mirror immediately above the specimen was transferred to a Czerny-Turner spectrograph, equipped with a 300 lines per mm (500 nm blaze) grating and a type R374 photomultiplier. Spectra were recorded digitally by scanning the wavelength from 200 to 900 nm, with a step size of 10 nm and a dwell time per step of 1 s. After background subtraction (based on the count-rate observed in the 200–250 nm region where the light intensity was zero), the spectra were corrected for the detection efficiency as determined with a standard tungsten lamp.

In order to investigate the effect of electron bombardment on the CL spectra, repeated wavelength scans were recorded for a typical agate. No changes in the wavelengths of the emission bands were observed, but the violet/red intensity ratio showed an increase from the first to the second scan equivalent to a relative violet enhancement of ~7% within a single wavelength scan. In the results reported below, an effect of this order can therefore be assumed. Where wavelength scans were repeated on nominally the same point, a small offset was applied to avoid the effect of previous electron bombardment.

Results

The curve-fitting algorithm in OriginLab's program *Origin* was used to fit Gaussian functions to the experimental spectra. In all cases, three such functions were fitted. The goodness of fit, shown by the coefficient of determination (r^2 ~0.97), was always better than with only two functions, even when the presence of a third band was not obvious from visual inspection. The positions and widths of the Gaussian functions were unconstrained. Examples of efficiency corrected plots of CL spectra are given in Fig. 2. The discussion is based on the relative peak intensities of these spectral emissions.

Three agates, ~3 cm in diameter, were selected to establish the size of CL variations within a

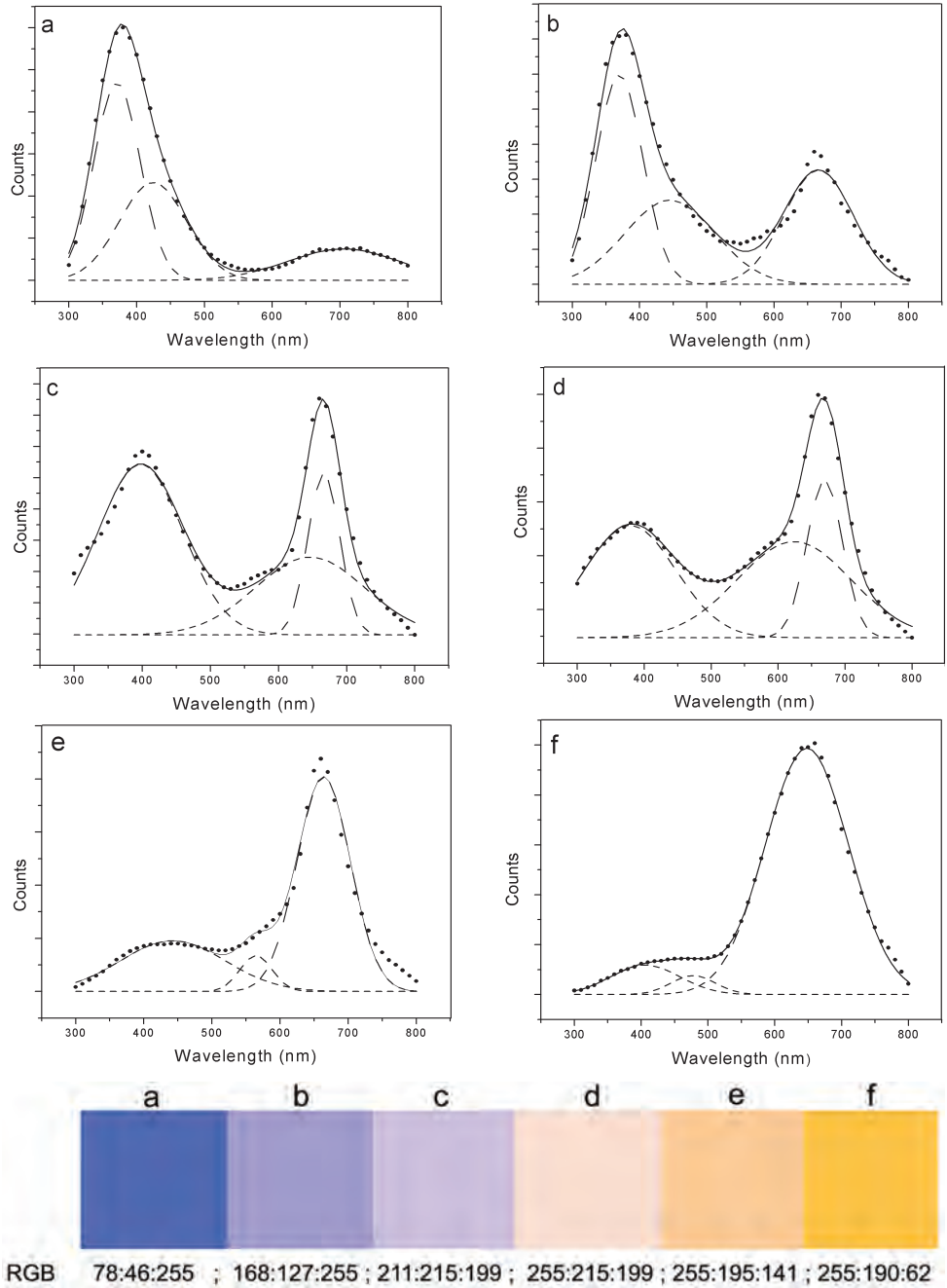

FIG. 2. Efficiency-corrected spectrum plots of igneous-hosted agates illustrating the range of colours found: (*a*) Brazil 64 (heated at 300ºC for 56 days); (*b*) Brazil 64 (heated at 300ºC for 35 days); (*c*) Brazil 31; (*d*) Lake Superior 12, USA; (*e*) Brazil 21; (*f*) Killara 6, Australia (solid circles – experimental data; dashed lines – fitted Gaussian components, with the sum shown by the solid line). The coloured squares and their respective RGB values refer to the spectra above as derived by means of the 'Calculate true colour' command in the Gatan Digital Micrograph software.

single agate. Agate from Parcelas, Mexico (38 Ma), Agate Creek, Australia (275 Ma) and Ethiebeaton, Scotland (412 Ma) were representative of the age range. Spectra were obtained from equidistant points positioned N→S and W→E in each agate. The CL spectra showed little difference between the relative intensities obtained within the agates. One exception was shown by CL spectra in the Parcelas sample where the spectra in the W→E direction were different from those obtained N→S. Here, the latter spectra were obtained from a more complex banding. In all samples the wavelengths of the emission bands at ~400 and 655 nm were similar but the mid-range colours were variable (Table 2).

In the main study, 236 spectra were obtained from >50 agates found in hosts aged 13−1100 Ma. Each spectrum produced emission bands at ~395(27) nm and ~662(12) nm. For the majority, a significant peak was also found in the mid-wavelengths at either 470(20), 565(15) or 622(16) nm. These wavelength peaks were found to be 16%, 52% and 30%, respectively, of the spectra scans (four scans were considered as outliers). The four random spectrum plots per agate have generally contained all three mid-range wavelengths but a few agates produced exclusively only one of the three available mid-range wavelengths. The following colour descriptions are used to describe the wavelengths (nm): violet − 395(27), blue − 470(20), yellow − 565(15), orange − 622(16), red − 662(12). The colours identified are due to different lattice defects and, unless stated to the contrary, are not interrelated.

Thin sections of agate show a variety of types of petrographic fibrosity in the clear areas. Additionally, the white bands in old agates (>100 Ma) show a plate-edge-like structure. The features were individually examined in a number of agates but CL was unable to discriminate between the observed petrographic differences. These additional scans were included when calculating the mean wavelengths and relative intensities.

The dehydration investigation of Brazil 60 and Brazil 64 showed that free and total water were 0.20% and 1.30%, and 0.21% and 1.22%, respectively. However, slab heating at 300ºC demonstrated that the water loss had stabilized after 14 days with mean losses of 38(±2)% and 66(±7)%, respectively, of the total available water.

Discussion

Variation in CL spectra with the age of the igneous host rock (13−1100 Ma)

The scans on the agates from hosts aged 13−1100 Ma were considered as three groups defined by a mid-range emission at 470(20), 565(15) and 622(16) nm. In order to establish whether there is a CL spectra-age dependency, the intensities were divided by host rock age at >100 Ma and <100 Ma.

Plots of the relative intensities of violet and red with mid-range blue or yellow were similar but it was not possible to distinguish between agates from host rocks of different ages. However, a plot of the relative intensities of violet, red and mid-range orange produces a lower relative orange intensity in the younger agates (Fig. 3). The mean value of the relative intensities of violet:orange:red are given by the older and younger agates as 33(8):33(8):34(8) and 36(7):23(6):41(8), respectively.

The relative intensities of separate violet, red, blue and yellow emissions from the blue or yellow sub-groups were plotted as a function of age and were found to be independent of age. Similar plots within the orange sub-group are shown in Fig. 4. Here, the violet emission (Fig. 4I) is also independent of age but an age dependency is shown by the red (Fig. 4II) and orange (Fig. 4III) emissions.

TABLE 2. Agate samples used for a preliminary investigation.

Agate region (age Ma)	Number of spectra/agate	Relative intensity Violet:mid-range:red colours	Wavelength (nm) Violet:mid-range:red colours
Parcelas, Mexico (38)	16	29(8):22(4):49(11)	404(15):568(41):659(6)
Agate Creek, Australia (275)	20	25(7):17(9):59(16)	414(15):566(23):650(9)
Ethiebeaton, Scotland (412)	11	34(10):23(7):43(14)	410(15):575(24):657(5)

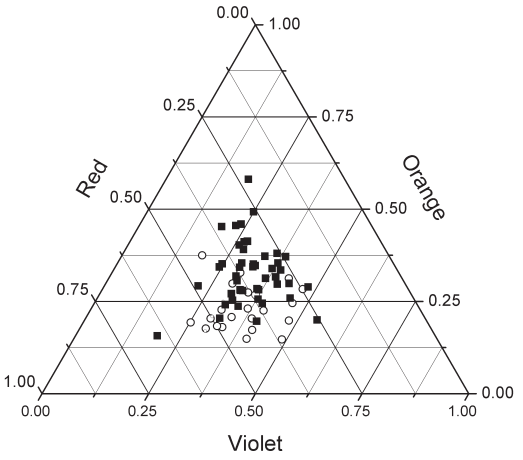

FIG. 3. The relative intensities of the violet, red and orange emission bands. Open circles and solid squares represent agate scans from hosts at <100 Ma and >100 Ma, respectively.

Thermogravimetric analysis on heated agate powders shows that loosely-bound water is lost up to 120ºC with minimal further water loss to 200ºC. Heating at higher temperatures removes tightly bound water and silanol water resulting in complete dehydration at 1000ºC (Yamagishi *et al*., 1997). The same study investigated the change in infrared spectra when agate was continuously heated over the 50−650ºC range. They found that the sharp peak at 3585 cm^{-1} (attributed to the silanol group, Graetsch *et al*., 1985) decreases continuously up to 650ºC. Moxon and Ríos (2004) investigated the defect-water loss as a function of age, and the plot, now given as log age, is shown in Fig. 4IV. A strong negative correlation is shown for the first ~400 Ma. After ~400 Ma the defect water in agate is approximately constant at ~0.4%. The change in mean relative intensity of the red emission shows a similar decrease and a link is proposed between the changes in this lattice defect and dehydration.

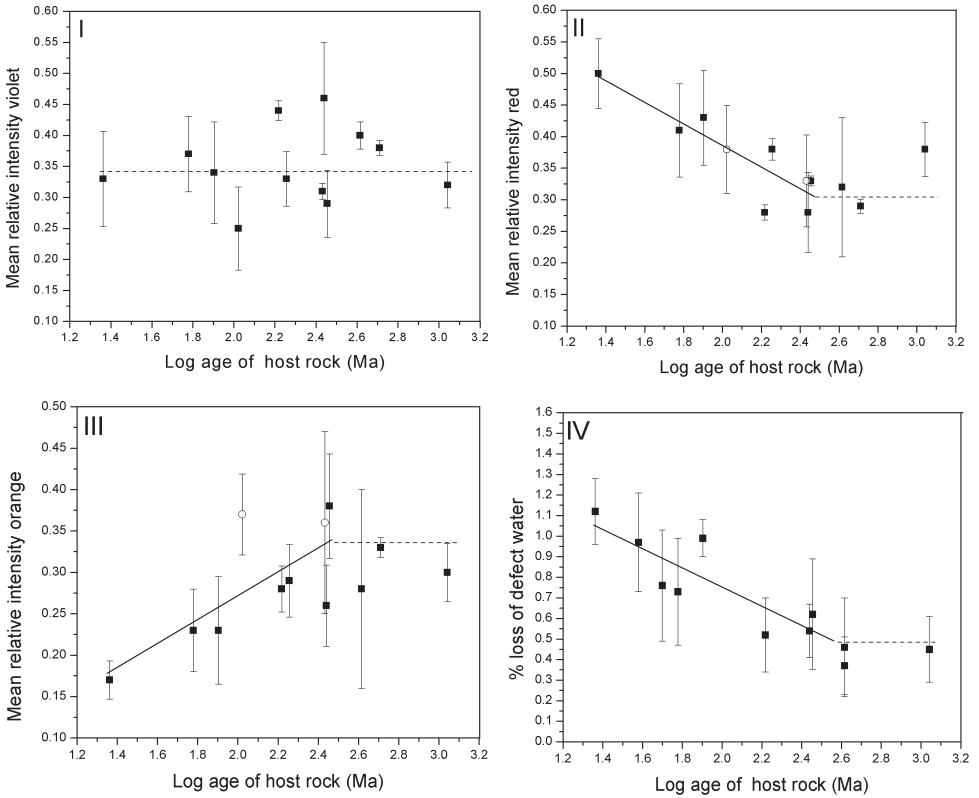

FIG. 4. (I, II, III) The mean relative intensities of the respective violet, red and orange emission bands. (IV) The loss of defect site water (data from Moxon and Rios, 2004). All plots as a function of log age. Open circles are agates from limestone hosts.

Furthermore, the rate of decrease in the mean red intensity (Fig. 4II) and the rate of increase in the mean orange intensity (Fig. 4III) have a similar magnitude in their respective gradients at −0.17 and 0.15.

The CL emissions in the 620 to 650 nm range found in quartz are attributed to the NBOHC with several possible precursors (Stevens Kalceff and Philips, 1995; Götze *et al*., 2001, and the literature therein). A likely precursor for the decreasing mean-relative intensity of the red emission (Stevens Kalceff and Philips, 1995) and the thermogravimetrically determined defect-site water loss (Moxon and Rios, 2004) is a condensation reaction between neighbouring silanol groups: $Si{-}O{-}H + Si{-}O{-}H \rightarrow Si{-}O{-}Si + H_2O$. Stevens Kalceff and Philips (1995) also propose a further precursor of the NBOHC as the strained Si−O bond when $\equiv Si{-}O{-}Si\equiv \rightarrow \equiv Si{-}O\cdot\ \cdot Si\equiv$. These changes offer valid explanations for the decreasing red and increasing orange emission bands. We propose that the decrease and growth of the respective 650 and 620 nm age-related emissions are due to the replacement of the silanol groups by a strained Si−O−Si bond.

Gíslason *et al*. (1997) demonstrated that the dissolution rate of moganite is 7.4 times faster than that of quartz at pH 3.5 and 25ºC. The total water contents of pure moganite and chalcedony are ~5% (Petrovic *et al*., 1996) and up to 2% (Graetsch *et al*., 1985), respectively. The defect-site water movement over the geological time scale would convert the lower-density moganite (2.55 g/cm^3, Miehe and Graetsch (1992)) into chalcedony and account for the age-related decrease in moganite and defect-site water accompanied by an increase in crystallite size and density (Moxon *et al*., 2006). Furthermore, it is proposed that the present study confirms that it is the silanol group and the subsequent condensation reaction that provides the necessary water for these changes.

Action of heat on Brazilian agate

Four slabs of Brazilian agate were furnace-heated at 300ºC in order to further examine agate dehydration. Three markers in each of the agates gave sites for repeated CL scans at 0, 35 and 56 days. The initial scans gave five mid-range emissions at 631(18) nm and seven at 574(3) nm. The changes in the relative intensities are shown in Fig. 5*a*. These changes on the 631 and 574 sites are tracked after 35 and 56 days and are shown in Fig. 5*a* – A, B and C. The precise positions were not re-tested and the new sites were changed marginally in order to avoid any effect of the previous electron bombardment.

Laboratory heating of Brazilian agate has produced changes in the mean relative intensities of the red, orange or yellow, and violet spectral emissions. However, a number of additional changes are not observed in agate maturing over geological time.

(1) A lattice defect resulting in an emission at 712(13) nm was formed after 56 days of heating at 300ºC (Fig. 5*b*,*c*). This band emission has not been observed in unheated agate.

(2) There is growth in the relative intensity of the violet emission band during the first 35 days of heating (Fig. 5*d*). In geologically maturing agate the violet band is independent of age.

(3) The decrease in the red emission band occurs within the first 35 days whereas the growth in the orange emission band is minimal in the first 35 days (Fig. 5*f*,*e*). The latter growth occurs mainly during days 35 and 56.

(4) Brazil 64 and Brazil 60 lost 66(7)% and 38(2)% of total water, respectively. The residual total water of Brazil 64 would be that of a 400 Ma agate.

The changing wavelengths of the emissions show that the heating heals existing defects and produces new defects that were not present in the original agate. The 574 and 630 nm initial emissions have been replaced by a 446(39) nm emission band after 35 days and a 430(8) emission band after 56 days (Fig. 5*c*). Likely causes of the 450 nm emission band are the oxygen vacancy or the twofold coordinated silicon defect (Stevens Kalceff, 1998, and references cited therein). A 470(20) nm emission band has been found in 16% of the agate scans in this study.

After 56 days of heating, a new lattice defect caused the development of a 712(13) nm emission band. This emission band has not been observed elsewhere in this study. A possible cause is the involvement of Fe^{3+} within the quartz lattice (Götze *et al*. (2001) and references therein). If Fe^{3+} is involved, then differences in ionic radii between Fe^{3+} and Si^{4+} mean that this can only occur at grain margins and at higher temperatures when the crystal lattice is widened

X-ray diffraction examination of these two Brazilian agates has shown that crystallite growth has not occurred over the 56 days of heating.

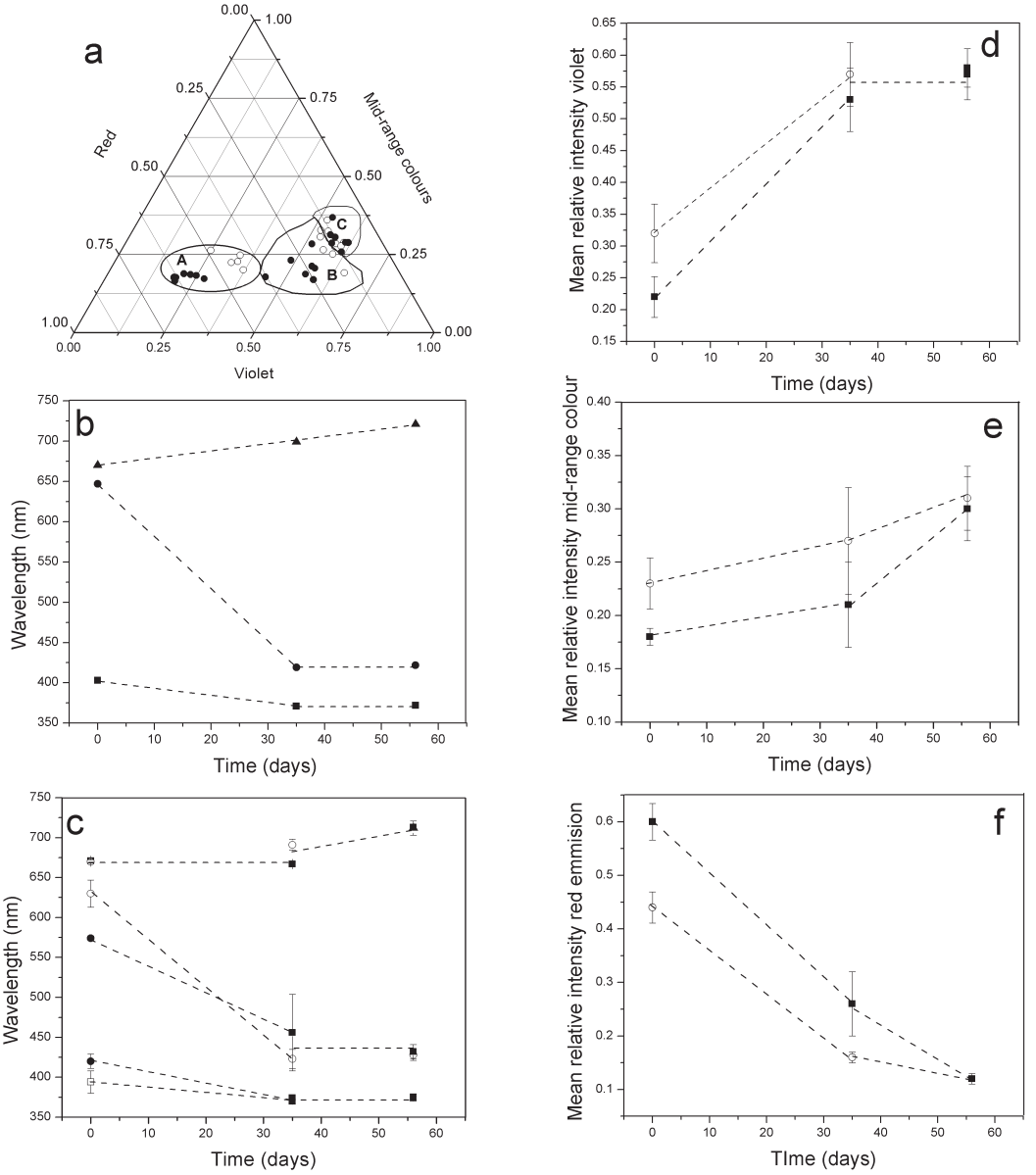

FIG. 5. The relative intensities of individual emissions from 12 spectra taken from four Brazilian agate slabs. (*a*) Data obtained at the start – A, B and C relative intensities after 35 and 56 days (open and solid circles show the respective intensities, and changes, from spectra showing initial mid-range emissions at 631(18) nm or 574(3) nm). (*b*) The changing wavelength as a function of time during the 56 day heating process based around a single hole in Brazil 64. Changes in the mean wavelength found in Brazil 60 and 64 (*c*). The changing mean relative intensities of the respective violet, orange or yellow, and red emissions during the 35 and 56 day heating (*d*, *e*, *f*). The 631 nm (open circles) and 574 nm (closed squares) are the starting mid-range wavelengths in *c*, *d*, *e* and *f*. Dashed lines are to help guide the reader's eye.

Nevertheless, heating at 300ºC has resulted in the continued decrease in the fraction of the emission band at 660 nm and the growth of the defect causing a 430 nm emission. One suggested origin of a similarly identified 420 nm wavelength emission is an intrinsic lattice defect (Stevens Kalceff and Philips, 1995). If this is the case, then the growth here is due to heating, as naturally maturing agate has shown that this defect is independent of age.

Agate from different host rocks and regions

It has been argued that a dominant yellow emission band that was regularly found in agates from acidic rocks (e.g. rhyolites) was linked to E'_1 centres (oxygen vacancy, Götze *et al*., 1999). A good correlation was found between the yellow emission and the abundance of E'_1 centres. This indicates a high concentration of lattice defects due to fast crystallization probably from a non-crystalline precursor (Götze *et al*., 1999). A plot showing individual scans from Brazilian agates (basalt host), agates from Mexico and Iran (andesite hosts), together with Fairburn agates and Lyme Regis chalcedony (limestone hosts) is given in Fig. 6. The relative intensities from the three hosts show only a very general distinction but each group has too many outliers for effective differentiation between different hosts. Various other hosts and groups have been investigated including Agate Creek agate (basalt host) and relative intensities using the orange emission band. In all cases, host differentiation has not been possible.

In addition, regional differences could not be demonstrated. Agates from Iran (12 wavelength scans on 3 agates), Botswana (17 wavelength scans on 4 agates) and Brazil (32 wavelength scans on 8 agates) produce similar relative intensities. The respective mean-relative intensities of violet, mid-range colour and red emission bands were {28(10), 21(6), 51(15)}; {29(6), 23(6), 48(9)} and {30(9), 20(6), 50(11)}. The inability of CL to distinguish between the mean-relative intensity of agates from different hosts and regions, demonstrates that agates share a common defect-site development during growth that is independent of host and region. However, other studies of agates from different igneous host-rocks using CL and electron paramagnetic resonance showed a clear difference between agates from basic and acidic rocks. Other defect types were found with different dominating CL emission bands. In some of the agates from Permian rhyolites, there was minimal red emission (650 nm) and only a strong emission band at ~580 nm (Götze *et al*., 1999).

Agate from hosts aged 1.84–3.48 Ga

Agates from three Western Australian regions were available for this study. The regions cover a wide range of geological time: Killara Formation (1.84 Ga host), the Maddina Basalt Formation (2.72 Ga) and the Warrawoona Group (3.48 Ga). All the host rocks show low-grade metamorphism and the change in the older rocks is probably due to burial during the Proterozoic: ~2.45 and 2.0 Ga (Nelson *et al*., 1992).

Warrawoona 1 is divided into four regions: milky macrocrystalline quartz (A), fibrous chalcedony (B), an area of transformation (C); and granular quartz (D). Agates always show developing growth from the outer edge to the centre and the arrows show the direction of growth in this agate (Fig. 7). Host burial metamorphism was proposed for the partial transformation of fibrous chalcedony to granular quartz (Moxon *et al.*, 2006).

Ghosts of fibrosity can just be observed in region C (Fig. 7) and any granularity will be best and least developed at areas g and R, respectively. A wavelength trend showing decreasing granularity or increasing proportion of chalcedony is not shown by the respective scans taken across

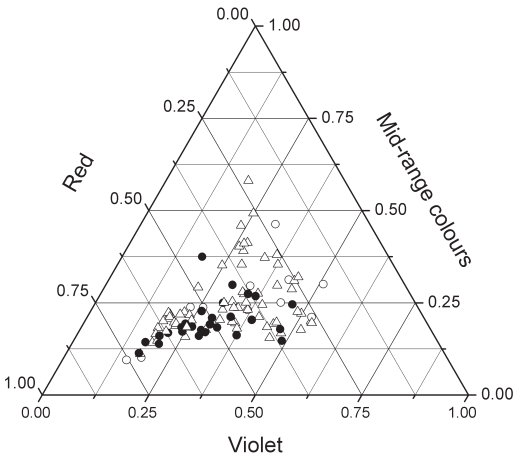

FIG. 6. Single scans on agates from Mexico and Iran (andesite hosts – open circles). Agates from Brazil (basalt hosts – solid circles). Fairburn agate and Lyme Regis chalcedony (limestone hosts – open triangles).

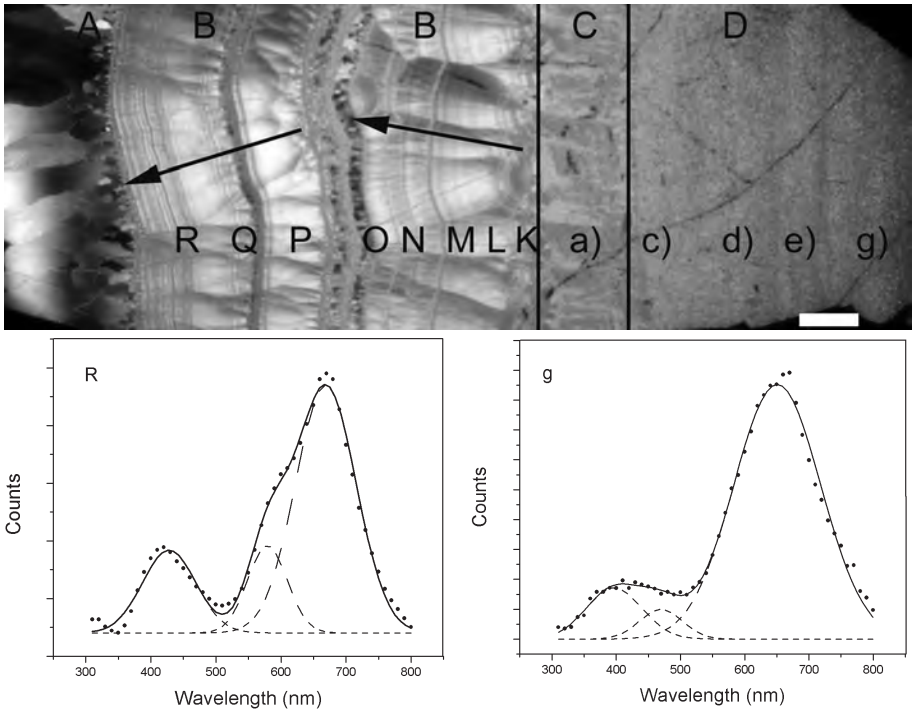

FIG. 7. Warrawoona agate 1. The agate is divided into four regions: milky quartz (A); fibrous chalcedony (B); transformation of fibrous chalcedony into granular quartz (C); granular quartz (D). The bold upper and lower case letters show the positions of CL scans in the chalcedony and granular region. The arrows show the direction of the original fibrous growth. g and R show emission bands in the respective granular and chalcedony regions. (Scale bar: 0.5 cm, polars crossed).

g→a and K→R (Fig. 7). However, there is a major difference between the CL scans in the chalcedony (R→K) and the granular region (g→a). The chalcedony transformation is accompanied by an increase in the red fraction shown by the mean relative intensities of the violet:mid-range:red fractions. The mean values determined for the chalcedony and granular quartz were 22(5):19(4):59(9) and 14(5):14(3):72(4), respectively. This chalcedony transformation is also matched by the healing and creation of lattice defects shown by the loss of the yellow peak (~560 nm) and a new blue emission band at 476(15) nm. The blue emission band has been found in some scans on younger agates and in the comparatively recently formed 1900 y old granular quartz sinter (Fig. 8). Note the minimal error bars that have been obtained for the mean of the scans on the mid-range emission band in these ancient agates.

The Killara (1.84 Ga) and Maddina (2.72 Ga) agates produce the 470 and 560 nm emission peaks, respectively. All the agates examined in this Proterozoic and Archaean group show an apparent fibrosity at low magnification but the fibrosity can be seen to be breaking down at higher magnifications. It is proposed that in the case of these mixed microstructures of partial transformation, the predominant peak is reflected by the proportion of granularity to fibrosity. Figure 8 suggests that the Killara samples have a greater proportion of granularity than fibrosity. This observation is confirmed by the relative peak intensities in Fig. 9 where the Maddina agate sits closer to the chalcedony of Warrawoona 1 while the Killara samples are linked with the region of granularity found in Warrawoona 1.

Conclusions

Chalcedony and agate from hosts that span 3480 Ma have been examined by CL. All CL scans of the agates examined have produced red and violet emissions together with either a blue,

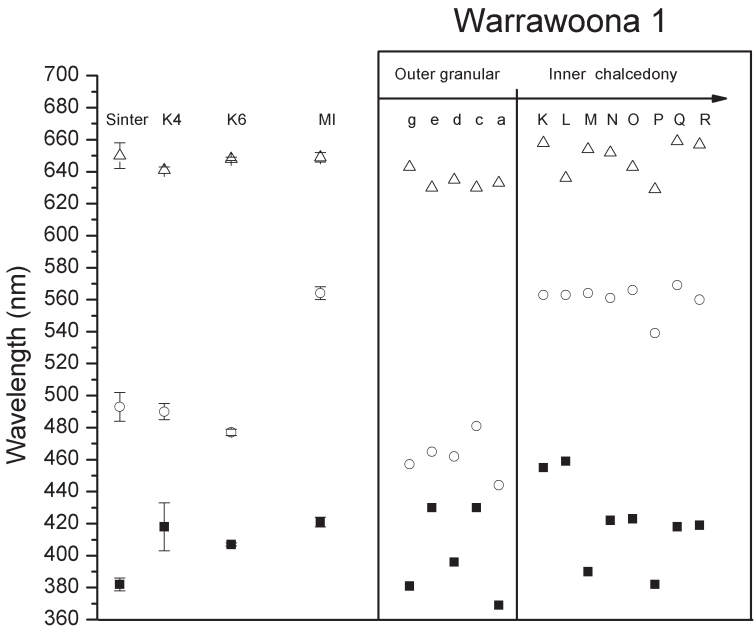

FIG. 8. Emission wavelengths shown by granular sinter (1900 y), and by Killara (1.84 Ga), Maddina (2.72 Ga) and Warrawoona (3.48 Ga) agates. Sinter, K4, K6 and M1 are the mean of four wavelength scans/agate. Warrawoona 1 shows the emission wavelengths from individual scans along the length of the agate. The upper and lower case descriptors are the positions of the CL scans shown in Fig. 7.

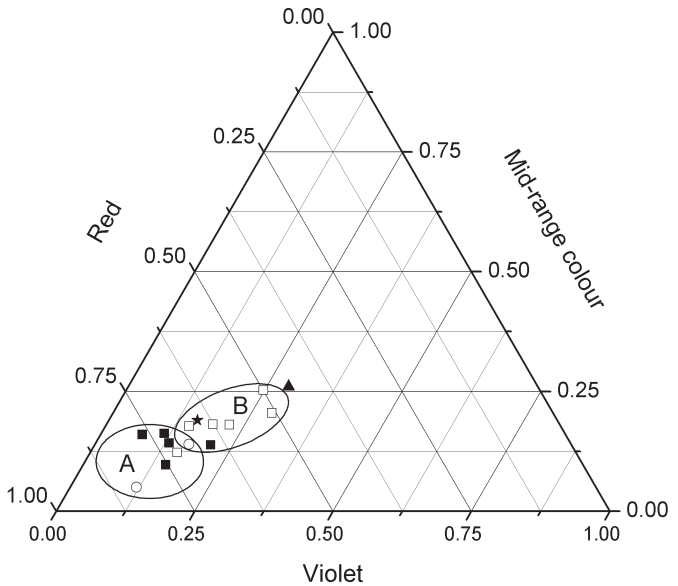

FIG. 9. The mean relative intensities found in Killara 6, Killara 4 (open circles), Maddina (star) agates and the granular sinter (triangle). The fibrous region of Warrawoona 1 (open squares) and granular region of Warrawoona 1 (closed squares) are shown as individual scans. Region A is predominantly granular. Region B is predominantly fibrous.

yellow, or orange mid-range emission band. These three mid-range emission bands are often found in the same agate. Less frequently, the exclusive mid-range emission band of blue or yellow or orange is identified in the same agate. Hence, it is likely that the causes of these lattice defects are present in all agates. The failure of CL to differentiate between agates from different regions and hosts suggests that agates share a common development of lattice defects during growth.

Only the red and orange emissions have been found to be age-related. The present study offers confirmation for the proposition that the red emission is due to a silanol precursor. Over the geological time scale, it is proposed that CL supports the hypothesis that neighbouring Si−OH groups (red emission band) eliminate water and form a strained Si−O−Si bond (orange emission band).

The Western Australian agates have been subjected to host-rock metamorphism and one agate has retained partial fibrosity as well as a conversion into granularity. The CL scans in this agate demonstrate that the transformation of fibrosity to granularity is accompanied by a change in the CL emission band from 560 to 476(15) nm due to the healing and creation of lattice defects. Laboratory-heated Brazilian agate has produced similar changes in CL emissions where mid-range emission bands at 630 and 574 nm produce a 446(39) nm emission band after 35 days of dry heating at 300ºC. Apart from these Western Australian samples, the exclusive production of the 460 nm emission from four scans per agate has been achieved in only one other sample. If CL scans on a collection of agates show only the universal red and violet emissions together with an exclusive ~460 nm emission band, then this could indicate palaeoheating within the surrounding parent rock.

Acknowledgements

This study has relied on the generous donation of chalcedony and agate specimens by collectors and research workers from around the world. We are grateful to Roger Clark, Nick Crawford, Brad Cross, Gerhard Holzhey, Herbert Knuettel, Reg Lacon, Brian Leith, Ian Lennon, Joe Moore, Maziar Nazari, Dave Nelson, Leonid Neymark, John Raeburn, John Richmond, Bill Taylor, Bill Wilson and Scott Wolter. We are also indebted to Michael Carpenter for discussions throughout the study, Ian Marshall for assistance with the SEM operation and Simon Galloway of Gatan Ltd. for carrying out an efficiency calibration of the spectrograph. We thank Jens Götze for constructive comments made after a first submission of this paper. TM thanks The Leverhulme Trust for financial support of these agate studies.

References

Clark, R. (2002) *Fairburn Agate Gem of South Dakota.* Silverwind Agates, Appleton, USA, 104 pp.

Flörke, O.W., Köhler-Herbertz, B., Langer, K. and Tönges, I. (1982) Water in microcrystalline quartz of volcanic origin: Agates. *Contributions to Mineralogy and Petrology*, **80**, 324−333.

Gíslason, S.R., Heaney, P.J., Oelkers, E.H. and Schott, J. (1997) Kinetic and thermodynamic properties of moganite, a novel silica polymorph. *Geochimica et Cosmochimica Acta*, **61,** 1193−1204.

Götze, J., Nasdala, L., Kleeberg, R. and Wenzel, M. (1998) Occurrence and distribution of 'moganite' in agate/chalcedony: a combined micro-Raman, Rietveld, and cathodoluminescence study. *Contributions to Mineralogy and Petrology*, **133**, 96−105.

Götze, J., Plötze, M., Fuchs, H. and Habermann, D. (1999) Defect structure and luminescence behaviour agate-results of electron paramagnetic resonance (EPR) and cathodoluminescence (CL) studies. *Mineralogical Magazine*, **63**, 149−163.

Götze, J., Plötze, M. and Habermann, D. (2001) Origin, spectral characteristics and practical applications of the cathodoluminescence (CL) of quartz − a review. *Mineralogy and Petrology*, **71,** 225−250.

Graetsch, H., Flörke, O.W. and Miehe, G. (1985) The nature of water in chalcedony and opal-C from Brazilian agate geodes. *Physics and Chemistry of Minerals*, **12**, 300−306.

Gries, J.P. and Martin, J.E. (1985) Composite outcrop section of the Paleozoic and Mesozoic strata in the Black Hills and surrounding areas. Pp. 261−292 in: *Geology of the Black Hills, South Dakota and Wyoming* (F.J. Rich, editor), American Geological Institute, Alexandria, Virginia, USA.

Heaney, P.J. (1993) A proposed mechanism for the growth of chalcedony. *Contributions to Mineralogy and Petrology*, **115**, 66−74.

Heaney, P.J. and Post, J.E. (1992) The widespread distribution of a novel silica polymorph in microcrystalline quartz varieties. *Science*, **255**, 441−443.

House, M. (1989) *Geology of the Dorset Coast.* The Geologists' Association, London, 170 pp.

Keller, P.C., Bockoven, N.T. and McDowell, F.W. (1982) Tertiary volcanic history of the Sierra del Gallego area, Chihuahua, Mexico. *Geological*

Society of America Bulletin, **93**, 303–314.

Lynne, B.Y., Campbell, K.A., Moore, J.N. and Browne, P.R.L. (2005) Diagenesis of 1900-year-old siliceous sinter (opal-A to quartz) at Opal Mound Roosevelt Hot Springs, Utah, U.S.A. *Sedimentary Geology*, **179**, 249–278.

Miehe, G. and Graetsch, H. (1992) Crystal structure of moganite: a new structure type for silica. *European Journal of Mineralogy*, **4**, 693–706.

Moxon, T. (2002) Agate: a study of ageing. *European Journal of Mineralogy*, **14**, 1109–1118.

Moxon, T. and Ríos, S. (2004) Moganite and water content as a function of age in agate: an XRD and thermogravimetric study. *European Journal of Mineralogy*, **16**, 269–278.

Moxon, T., Nelson, D.R. and Zhang, M. (2006) Agate recrystallization: evidence from samples found in Archaean and Proterozoic host rocks, Western Australia. *Australian Journal of Earth Sciences*, **53**, 235–248.

Nelson, D.R., Trendall, J.R., de Laeter, J.R., Grobler, N.J. and Fletcher, I.R. (1992) A comparative study of the geochemical and isotopic systematics of late Archaean flood basalts from the Pilbara and Knaapvaal cratons. *Precambrian Research*, **54**, 231–256.

Petrovic, I., Heaney, P.J. and Navrotsky, A. (1996) Thermochemistry of the new silica polymorph moganite. *Physics and Chemistry of Minerals* **23**, 119–126.

Stevens Kalceff, M.A. (1998) Cathodoluminescence microcharacterization of the defect structure of irradiated hydrated and anhydrous fused silicon dioxide. *Physical Review B*, **57**, 5674–5683.

Stevens Kalceff, M.A. and Philips, M.R. (1995) Cathodoluminescence microcharacterization of the defect structure of quartz. *Physical Review B*, **52**, 3122–3134.

Yamagishi, H., Nakashima, S. and Ito, Y. (1997) High temperature infrared spectra of hydrous microcrystalline quartz. *Physics and Chemistry of Minerals*, **24**, 66–74.

[*Manuscript received 13 June 2006: revised 14 October 2006*]